Quaternary Science Reviews 228 (2020) 106087

Contents lists available at ScienceDirect

Quaternary Science Reviews

journal homepage: www.elsevier.com/locate/quascirev

+A 5680-year tree-ring temperature record for southern South America

A. Lara [a, b, c, *], R. Villalba [d], R. Urrutia-Jalabert [e, b, a], A. González-Reyes [f, b, a], J.C. Aravena [g], B.H. Luckman [h], E. Cuq [a], C. Rodríguez [a], A. Wolodarsky-Franke [i]

[a] Laboratorio de Dendrocronología y Cambio Global, Instituto de Conservación, Biodiversidad y Territorio, Facultad de Ciencias Forestales y Recursos Naturales, Universidad Austral de Chile, Valdivia, Chile
[b] Center for Climate and Resilience Research (CR)^2, Santiago, Chile
[c] Fundación Centro de los Bosques Nativos FORECOS, Valdivia, Chile
[d] Instituto Argentino de Nivología, Glaciología y Ciencias Ambientales (IANIGLA-CONICET), Mendoza, Argentina
[e] Instituto Forestal (INFOR), Fundo Teja Norte S/N, Valdivia, Chile
[f] Hémera Centro de Observación de la Tierra, Facultad de Ciencias, Universidad Mayor, Santiago, Chile
[g] Centro de Investigación Antártica, Universidad de Magallanes, Punta Arenas, Chile
[h] Department of Geography, University of Western Ontario, London, Ontario, Canada
[i] Cooperativa Calahuala, Valdivia, Chile

ARTICLE INFO

Article history:
Received 23 July 2019
Received in revised form
15 November 2019
Accepted 16 November 2019
Available online xxx

Keywords:
Holocene
Paleoclimatology
South America
Tree-rings

ABSTRACT

It is widely documented that the Earth's surface temperatures have increased in recent decades. However, temperature increment patterns are not uniform around the globe, showing different or even contrasting trends. Here we present a mean maximum summer temperature record, based on tree-ring widths, over the past 5682 years (3672BC – 2009AD) for southern South America (SSA), covering from mid-Holocene to the present. This is the longest such record for the Southern Hemisphere (SH), and expands available annual proxy climate records for this region in more than 2060 years. Our record explains 49% of the temperature variation, and documents two major warm periods between 3140 –2800BC and 70BC – 150AD, which coincide with the lack of evidence of glacier advances in SSA. Recent decades in the reconstruction (1959–2009) show a warming trend that is not exceptional in the context of the last five millennia. The long-term relationship between our temperature reconstruction and a reconstructed total solar irradiance record, with coinciding cycles at 293, 372, 432–434, 512 and 746 years, indicate a persistent influence of solar forcing on centennial climate variability in SSA. At interannual to interdecadal scales, reconstructed temperature is mainly related to the internal climate variability of the Pacific Ocean, including El Niño Southern Oscillation (ENSO) and longer oscillations. Our study reveals the need to characterize regional-scale climate variability and its drivers, which in the context of global-scale processes such as anthropogenic warming, interact to modulate local climate affecting humans and ecosystems.

1. Introduction

It is widely accepted that the Earth surface temperatures have increased in recent decades compared with the last several centuries (Masson-Delmotte et al., 2013; Pages 2k Consortium, 2013). However, this warming pattern is not uniform, with substantial differences between regions. For example, there are no clear temperature trends during recent decades in southwestern South America between 38° and 48°S (Falvey and Garreaud, 2009; Hartmann et al., 2013). Although a moderate warming occurred during the 20th century in southern Chile between 39° - 44° S (Lara and Villalba, 1993; Urrutia-Jalabert et al., 2015a; Villalba et al., 2003; Vuille et al., 2015), a cooling trend has been reported along the Pacific coast (17° – 37° S) of South America for the periods 1979–2006 and 1981–2012 (Falvey and Garreaud, 2009; Hartmann et al., 2013).

Recognition and attribution of the causes of temperature

* Corresponding author. Laboratorio de Dendrocronología y Cambio Global, Instituto de Conservación, Biodiversidad y Territorio, Facultad de Ciencias Forestales y Recursos Naturales, Universidad Austral de Chile, Valdivia, Chile.
E-mail address: antoniolara@uach.cl (A. Lara).

https://doi.org/10.1016/j.quascirev.2019.106087

fluctuations depend on the quantification of the spatial and temporal variations in surface temperatures (Anchukaitis et al., 2017; Hegerl et al., 1997; Stott and Jones, 2009). Long annually resolved proxy temperature records are key to distinguish natural climate variability from recent human-induced climate changes (Hegerl et al., 2007, 2003). In the temperate Northern Hemisphere (NH), records for the last millennium and longer periods are dominated by tree-ring reconstructions and include other proxy records from a dense and robust network of sites (e.g. Anchukaitis et al., 2017; Pages 2k Consortium, 2013; Wilson et al., 2016). In contrast, long, annually resolved, temperature reconstructions from tree-ring records for the ocean-dominated Southern Hemisphere are restricted to a few records. Millennial temperature reconstructions have been developed for Tasmania (1600 BC- 2001 AD), New Zealand (900–1999 AD; Cook et al., 2006), for the eastern slopes of the Patagonian Andes in Argentina (860–1984 AD; Villalba, 1990), and for southern Chile covering the last 3620 years (Lara and Villalba, 1993). More recently, a multiproxy temperature record for southern South America spanning 1000 years, has also been developed by Neukom et al. (2011). Shorter tree-ring based temperature reconstructions in southern South America (SSA) start in 1600 AD (Villalba et al., 2003) and 1800 AD (Aravena et al., 2002; Lavergne et al., 2018).

At present, the various paleo-temperature records from SSA show discrepancies, consisting in some cases with different trends in instrumental records (Falvey and Garreaud, 2009; Villalba et al., 2003). Some indicate unprecedented temperature increase in recent decades compared with the last centuries that might be attributed to climate change (Lavergne et al., 2018; Villalba et al., 2003). Conversely, other studies document that the recent temperature increase is within the long-term range of climate variability (Elbert et al., 2015; Lara and Villalba, 1993). In order to characterize the long-term patterns of climate variability in SSA, there is a need to provide new robust multi-millennial, annually resolved, temperature records that enhance the low-frequency variability in climate. The large conifer *Fitzroya cupressoides* (alerce), that grows in Southern Chile and locally in adjacent Argentina for up to 3600 years (Lara and Villalba, 1993), offers a unique opportunity to develop such long-term climate records.

Understanding the temporal patterns of multi-millennial temperature variations in the SH is crucial for the comprehension of recent global trends and their ocean-atmosphere circulation drivers (Neukom et al., 2014; Trenberth et al., 2014). Incoming solar radiation, overlapped with internal modes of coupled ocean-atmosphere variability (e.g. El Niño Southern Oscillation, ENSO) can influence temperature anomalies at different spatial and temporal scales (Anchukaitis et al., 2017). Solar radiation has been documented as an important driver of low frequency (centennial) temperature and tree-ring growth variability over a broad geographic area in the Northern Hemisphere during the last millennia (Anchukaitis et al., 2017, 2013; Breitenmoser et al., 2012). Similarly, solar activity represented by the 80-year Gleissberg cycle, has been described as a potential driver of low-frequency climate and tree-ring variability in SSA (Lara et al., 2008; Muñoz et al., 2016; Roig et al., 2001; Villalba et al., 1996). At shorter time scales (interannual to interdecadal), other forcings such as the Southern Annular Mode (SAM), El Niño Southern Oscillation (ENSO) and the Pacific Decadal Oscillation (PDO) have been reported as important drivers of climate variability and tree-growth during recent centuries in SSA (Christie et al., 2011; Lara et al., 2015; Villalba et al., 2012).

Within this context, this study addresses the following questions: 1) How has temperature fluctuated in SSA during the last millennia? 2) How do temperature trends since 1900 and in recent decades compare with those during the last millennia? and 3) What are the main forcings of long-term temperature variations at interannual to multicentennial scales in SSA?

2. Methods

2.1. Study area

The study area includes eight *Fitzroya cupressoides* sites located in the Andean Range of North Patagonia in Chile (41° 32′- 42° 20), at elevations ranging from 700 to 1010 m. a.s.l. (Fig. 1 and Table 1 in the Supporting Information). It has a temperate wet oceanic climate with a mean annual temperature between 5.5 and 7.1 °C and annual rainfall between 4000 and 6600 mm (Urrutia-Jalabert et al., 2015a). Topography at the sampling sites varies from gentle (10° - 15°) to relatively steep slopes (up to 25°). Soils in the study sites developed from andesitic volcanic deposits such as tephra, are acidic, 0.5–1 m deep with a high organic matter content and silty loam in texture. They have a high C/N ratio indicating low decomposition rates and high exchangeable aluminum content making limited nutrients even less available (Urrutia-Jalabert et al., 2015a,b). Forest stands are dense or semi-dense (crown cover > 50%), dominated by the large conifer *Fitzroya cupressoides*, mixed with variable proportions of broadleaved evergreen species such as *Nothofagus betuloides*, *N. nitida, Laureliopsis philippiana* and the conifer *Saxegothaea conspicua*, among others. These sites are remote, accessible only by hiking and were selected primarily due to the presence of large (diameter at breast height between 80 and 280 cm) *Fitzroya* trees and the lack of evidence of human disturbances (e.g. fire, logging, grazing). The Lenca (LEN) site was selectively logged in 1976. In order to exclude this influence on tree growth, tree ring series for this particular site were used only until 1975, whereas series in all other sites were used until the sampling dates indicated in Table 1.

2.2. Tree-ring records and chronology development

Increment cores from living trees, as well as cross-sections and wedges from subfossil snags buried by deep tephra layers at site PTB, were collected in several field campaigns between 1994 and 2011. We collected two samples per tree in eight sites (Fig. 1, Table 1). Cores and sections were sanded, and tree-rings were measured to the nearest 0.001 mm, crossdated to verify the assignment of a calendar year to each ring in every sample and standardized using standard dendrochronological techniques (Fritts, 1976; Holmes, 1983; Stokes and Smiley, 1968).

Starting dates of the site chronologies varied between 3672 BC and 772 AD, and ending dates between 375 BC and 2010 AD (Table 1). Site chronologies were significantly correlated ($P < 0.05$) for the common period 772–1975 AD (Table S1). Therefore, a composite chronology (named Andean Composite Chronology, COM) covering the period 3672 BC – 2009 AD (5682 years), was developed by combining all the 481 radii collected in the eight sites (Table 1).

Non-climatic variability from tree-ring series, such as the typical decline in ring width due to the increase in age was removed through standardization (Fritts, 1976). The *Fitzroya* composite chronology was standardized by fitting age-dependent splines with an initial value of 50 years to individual ring widths and detrending the series using the 'signal free' (SF) method (Melvin and Briffa, 2008). In each series, tree-ring widths were divided by the value estimated by this age-dependent spline for each year and transformed to non-dimensional tree-ring indices using the software developed by Ed Cook (RCSigFree; Cook, 2017). The SF method is designed to enhance the preservation of common medium-to-long term frequency variance (timescales from multidecadal to centennial or more) in the tree-ring series. In addition, the use of

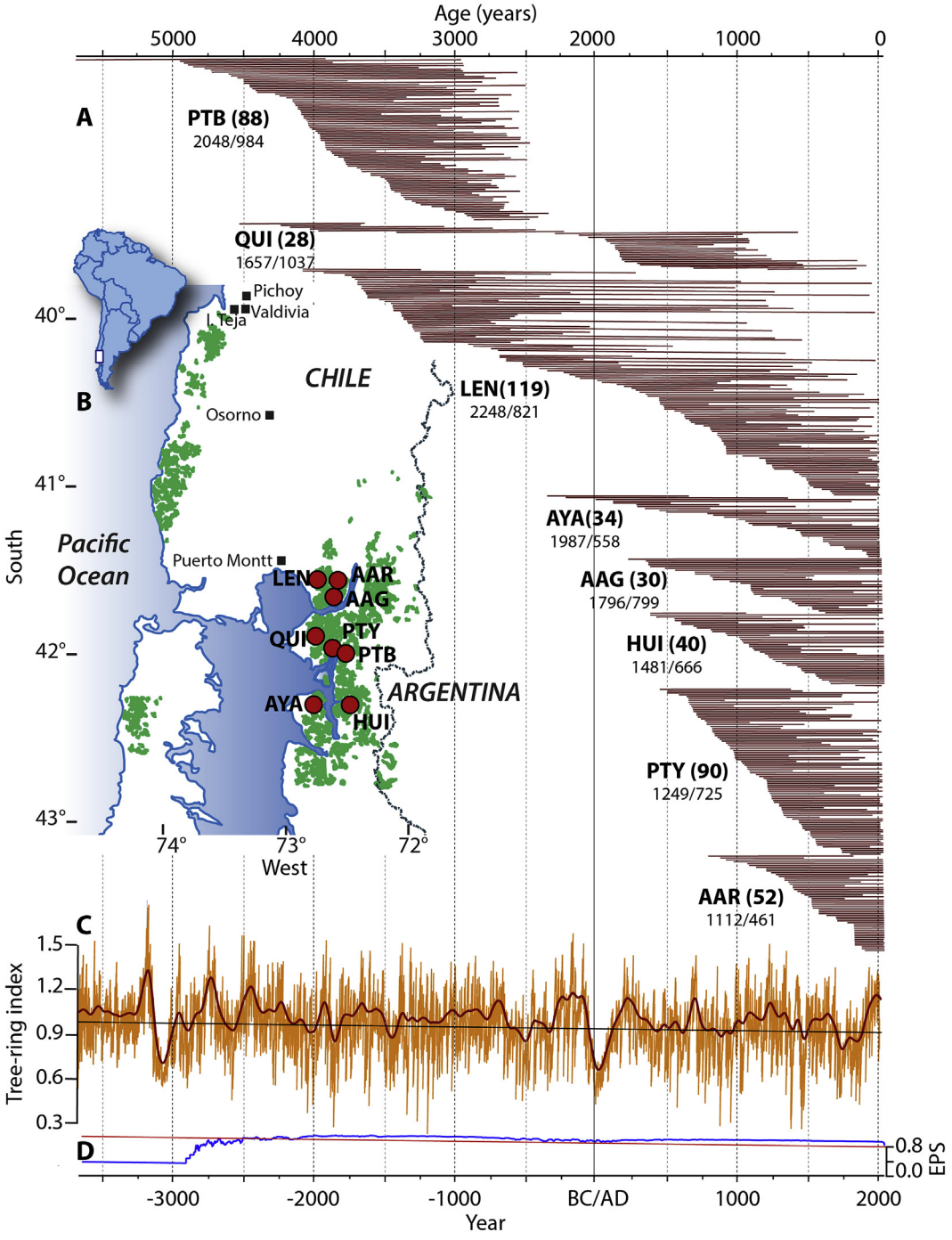

Fig. 1. (A) Temporal extent of individual tree-ring series within each *Fitzroya* tree-ring chronology: PTB: Patamay buried, QUI: Quildaco, LEN: Lenca, AYA: Ayacara, AAG: Alerce Andino Gaviotas, HUI:Huinay, PTY: Patamay, AAR: Alerce Andino. Numbers in parentheses correspond to the number of series in each chronology and the numbers below separated by a slash correspond to the maximum and median length of the series, respectively; (B) Map of southern Chile showing the location (red circles) of the eight tree-ring chronologies that form the Andean composite chronology and the location (black Squares) of the weather stations used. *Fitzroya* forests are shown in green. The location of the study area is indicated on the blue inset map; (C) Andean composite tree-ring chronology spanning the period 3672 BC– 2009 AD (5682 years), with a 128-year spline filter (thick dark line) to highlight the low frequency variability; (D) Expressed Population Signal (EPS; (Briffa and Jones, 1990) of the composite tree-ring chronology, showing values $\geq$ 0.85 since 2328 BC. On top, age (years) counted from 2019 to facilitate comparisons with ^{10}Be dated moraines for glacier records (e.g. Kaplan et al., 2016; Strelin et al., 2014). (For interpretation of the references to colour in this figure legend, the reader is referred to the Web version of this article.)

the SF method reduces the "trend distortion" effect during the detrending of the tree-ring series. This distortion effect, which is caused by the influence of common persistent medium-frequency signals on the fitting of the detrending curves (Melvin and Briffa, 2008), is most prevalent at the ends of the chronologies. This SF skill is particularly relevant for the standardization of the *F. cupressoides* composite chronology, since the observed recent increase in radial growth must be accurately determined. The Regional Curve Standardization method has been proposed to detrend chronologies that include subfossil material (Cook et al., 1995). In our case the SF method performed better than the RCS to correct for the loss of common variance and facilitated the

Table 1
Location and characteristics of each *Fitzroya* collection used to develop the Andean composite tree-ring chronology (COM) shown at the bottom.

Code	Site	Latitude/Longitude (S) W)	Elevation (m.a.s.l.)	Period[b]		Number of years	No of radii	No of trees	Source
PTB	Patamay Buried	41°52′/72°31′	750	−3672	−345	3328	88	59	This Study
QUI	Quildaco	41°51′/72°38′	872	−2537	1918	4456	28	25	This Study
LEN[a]	Lenca	41°33′/72°35′	740	−2082	2001	4084	119	112	Lara and Villalba (1993)
AYA	Ayacara	42°16′/72°45′	700	−354	1993	2348	34	23	Lara et al. (2000)
AAG	Alerce Andino Gaviotas	41°39′/72°36′	780	205	2000	1796	30	27	This Study
HUI	Huinay	42°20′/72°24′	1010	356	2007	1652	40	37	This Study
PTY	Patamay	41°52′/72°31′	750	448	2009	1562	90	70	This Study
AAR	Alerce Andino	41°32′/72°35′	760	772	2010	1239	52	48	Urrutia-Jalabert et al. (2015a)
COM	Andean Composite	–		−3672	2009	5682	481	401	This Study

[a] Considered until 1975 for the Composite Chronology.
[b] Negative numbers correspond to years BC.

preservation of oscillations longer than the lengths of the tree-ring series used for the chronology development (Melvin and Briffa, 2008).

The quality of the composite chronology was assessed using the Expressed Population Signal (EPS) statistic (Briffa and Jones, 1990), using a 50-year window with a 25-year overlap. EPS is a measure of the correlation between the average of a finite number of tree-ring series and a hypothetical chronology that has been infinitely replicated and assumed to represent the population (Briffa and Jones, 1990). EPS values above or close to 0.85 are considered an indication of robust tree-ring chronologies regarding temporal stability, good quality and a strong common signal (Wigley et al., 1984).

2.3. Temperature instrumental records

A regional monthly mean maximum temperature record (1959–2009) was created averaging the standardized departures of four highly correlated stations located in southern Chile: Pichoy Airport Valdivia, Universidad Austral Valdivia, Cañal Bajo Osorno and El Tepual Puerto Montt (Fig. 1, Tables S2–S4). These records were selected because they represented the best combination of proximity to the study sites, length, completeness, and reliability of the climate records. The common period to calculate the standardized deviations was 1966–2006. In addition, we also used the monthly mean temperature data recorded by Carlos Anwandter for Isla Teja Valdivia, which is the oldest instrumental temperature record in southern Chile for the period March 1851 through March 1883 (Table S2).

2.4. Chronology adjustment due to atmospheric CO_2 increase

Currently, there is abundant evidence of the positive effect of higher atmospheric CO_2 concentration on tree growth in various sites worldwide. A strong CO_2 fertilization effect has been the main explanation for the significant increase in water-use efficiency (WUE) reported for Northern Hemisphere temperate and boreal forests over the recent two decades (Keenan et al., 2013). Several studies have documented that CO_2 fertilization has a positive effect on radial growth rates through an increase in WUE (e.g. Camarero et al., 2015; R. Huang et al., 2017; Koutavas, 2013; Martínez-Vilalta et al., 2008; Song et al., 2019; Soule and Knapp, 2006, among others). Nevertheless, increased WUE does not always lead to enhanced tree growth (Lévesque et al., 2014). It has been reported that isotope discrimination (which depicts the variability resulting only from physiological responses to environmental change) in combination with the analysis on intrinsic water-use efficiency (iWUE), can be used together with tree-growth to detect CO_2 fertilization on forest ecosystems (Silva and Anand, 2013; Silva and Horwath, 2013).

Fitzroya tree-ring growth is negatively correlated with previous summer temperature (Lara and Villalba, 1993; Urrutia-Jalabert et al., 2015a; Villalba, 1990), and despite of this, its growth has been increasing since the 1900s (Fig. S1). This trend, also documented by Urrutia-Jalabert et al. (2015a), is unexpected due to the moderate increase in observed summer temperature in Southern Chile since the 1970s (Fig. 3B).

A $\delta^{13}C$ stable isotope tree-ring chronology developed for *Fitzroya* in one of the sites of our study (AAR Fig. 1, Table 1) showed a significant decreasing trend in carbon isotope discrimination since the 1900s and a steep increase in iWUE (Urrutia-Jalabert et al., 2015a). The increasing growth trend and decreasing isotope discrimination in *Fitzroya* have been attributed to a raise in photosynthetic rates, which has been caused by increased CO_2 and/or higher surface radiation, the latter associated with a reduction in cloudiness in a high precipitation area (Urrutia-Jalabert et al., 2015a). In the eastern slope of the northern Patagonian Andes, Argentina, under lower rainfall and cloudiness than in the Chilean western slope, a marked increase in *Fitzroya* tree-ring growth during the 20th century has also been recorded and attributed to increased CO_2 concentration (Lavergne et al., 2018). The coincident *Fitzroya* growth patterns in two areas of contrasting cloud cover is an additional support for the attribution of CO_2 fertilization in this species. Consistently, it has been recently reported that increasing WUE trends in tree-rings due to rising atmospheric CO_2, have been mostly produced by enhanced photosynthesis in mesic sites, rather than by reductions in stomatal conductance that are more widespread in sites with moisture limitations (Guerrieri et al., 2019).

Any potential atmospheric fertilization effect on forests must be considered in the calibration of tree-ring based climate reconstructions, since important biases related to amplitudes and trends in reconstructed variables may arise, or even low frequency and long-term trends might be lost from these records (Scharnweber et al., 2019). The increasing trend in *Fitzroya* tree-ring growth that occurs under rising temperatures during recent decades is contradictory due to the negative temperature response of this conifer. This justifies the need to adjust the *Fitzroya* chronology by removing the effect of CO_2 fertilization on radial growth. Consequently, we developed a reconstruction from the *Fitzroya* tree-ring chronology adjusted for the effect of CO_2 fertilization, and tested its suitability against a reconstruction based on the non-adjusted chronology.

There are three different gas-exchange responses of plants to the increase in CO_2, which can be studied using carbon isotopes in tree rings (Saurer et al., 2004). These scenarios differ in the magnitude to which the increase in internal carbon (Ci) follows the increase in ambient carbon (Ca) and are: (1) no response, (2) proportionally or (3) at the same rate (Saurer et al., 2004). The most common observed response of forests worldwide to changing atmospheric CO_2 concentration follows scenario (2), which implies

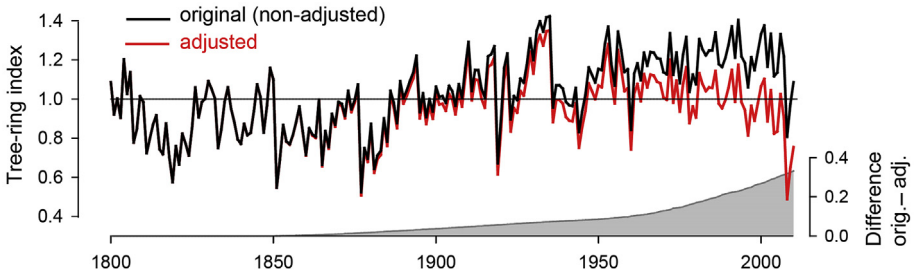

Fig. 2. Original (non-adjusted) chronology and adjusted composite tree-ring chronology considering the removal of the effect of CO_2 increase on tree-growth for the 1800–2009 period. Prior to 1861 both records are identical.

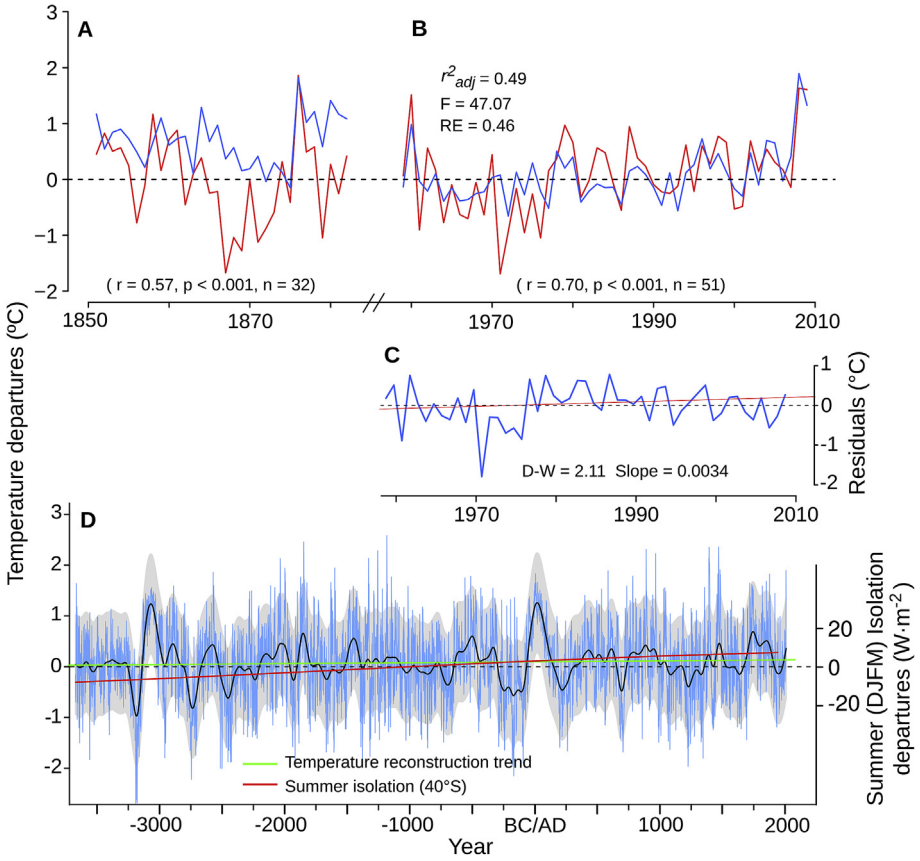

Fig. 3. (A) Comparison between the observed mean summer temperature recorded by C. Andwanter for Isla Teja, Valdivia (red line) and the reconstructed mean maximum summer temperature (blue line) for the period 1852–1883; (B) Observed regional average (red) and reconstructed (blue) mean maximum summer temperature for the period 1959–2009. Statistics of the reconstruction are shown (F-value of the regression model; RE: reduction of error); (C) Variation in the residuals of the reconstruction showing a non-significant slope and a Durbin-Watson statistic (D–W) close to 2; (D) Mean maximum summer temperature tree-ring reconstruction for the period 3672 BC–2009 AD and associated uncertainty bands (grey areas) corresponding to twice the standard error of the reconstruction. A 128-year spline filter has been added in black and the overall trends of the temperature reconstruction and summer insolation intensity at 40° S (Berger and Loutre, 1991). (For interpretation of the references to colour in this figure legend, the reader is referred to the Web version of this article.)

that the Ci/Ca ratio stays constant with a moderate increase in water use efficiency (Frank et al., 2015; Urrutia-Jalabert et al., 2015a).

In order to remove the positive trend in the tree-ring width chronology due to the increase in atmospheric CO_2 concentration, we calculated the iWUE under scenario (2). The initial Ci value for 1850 was calculated as the mean of the 1800–1850 values from the $\delta^{13}C$ isotope chronology for the AAR site (Urrutia-Jalabert et al., 2015a, Table 1). The new iWUE series covering the 1850–2010 period was subsequently used to discount the CO_2 effect on tree-growth. The iWUE values were transformed to tree growth units using the following approach. Regression analyses were performed between tree-ring index and summer (December–March) mean maximum temperature, considering different moving 20-year calibration periods lagged 1 year over the common interval 1959–2009 (Fig. S2). For those regression models in which the R^2 explained by December–March mean maximum temperature was >0.25, the regression equations were used to predict growth in the remaining 31-year period (Fig. S2). Differences between mean observed and predicted growth values were calculated for consecutive 20-year periods and these differences related through a regression to the differences in mean iWUE between the same

periods. The regression was forced to an intercept equal to zero and the slope of the regression (0.012) was the value used to multiply the increment in iWUE since 1850. This increment in iWUE, finally transformed to tree-growth, was subtracted from the tree-ring chronology in order to obtain the "adjusted chronology" after removal of the CO_2 increase effect (Fig. 2). This procedure is somewhat more elaborated than the one used by Lavergne et al. (2018), where the determination of the "extra" growth by CO_2 fertilization took into account the direct effect of the increase of iWUE.

2.5. Temperature reconstruction

Previous studies have demonstrated that summer temperature is the main climate driver of tree-ring growth in *Fitzroya* (Lara and Villalba, 1993; Villalba, 1990). We correlated the adjusted and non-adjusted composite chronologies with different combinations of monthly mean and maximum temperature of the current and previous years. (Table S5).

The reconstruction equation was estimated by regressing December–March mean maximum temperatures and tree-ring indices from the Andean composite chronology. The entire common period (1959–2009) between tree-ring and temperature records was used to calibrate the tree-ring model utilizing the "leave-one-out" cross-validation procedure (Meko, 1997; Michaelsen, 1987). In this method, each observation is successively withdrawn; a model is estimated on the remaining observations, and a prediction is made for the omitted observation. The application of this method does not affect the lagged relationship because the value taken for verification each time is withheld in a pair-wise manner (e.g., tree ring 1990 and temperature 1991). This method was selected because it is adequate especially when climate records are relatively short, in our case covering the 1959–2009 period. The proportion of variance explained by the regression or adjusted R^2 (R^2_{adj}) was used to evaluate the quality of fit between the observed and predicted values. F-value of the regression, reduction of error (RE) and the Durbin–Watson test (Ostrom, 1990), were used to assess the robustness of the reconstruction model.

2.6. Temperature forcings from centennial to multicentennial scales

We compared our temperature reconstruction with a multi-proxy reconstruction of Total Solar Irradiance (TSI) estimated every 22 years since 9400 BP (Steinhilber et al., 2012). The TSI record is based on three main high-resolution proxies: two ^{10}Be ice core records and a global p^{14}C (^{14}C production rate measured in tree rings from a network including sites in different regions) covering the period from 9400 to 1194 BP. The period starting thereafter (corresponding to 757 AD), was covered by seven proxies of different length (Steinhilber et al., 2012).

Visual comparison between the temperature and TSI reconstructions, reveals several coincidences in negative departures, with a pattern of an increasing offset between both records with younger ages for the TSI record than the temperature reconstruction (Fig. S4A). From this visual comparison, we noticed that these offsets started back of 757 AD and were ~20 years for the 440–1440 AD period, ~80 years for 850 BC – 150 AD and ~130 years for the 3420–2420 period (Fig. S4B). Steinhilber et al. (2012) indicated the presence of several sources of systematic errors in the dating of the TSI record, including uncertainties in the temporal scales of the individual records used to generate the composite TSI reconstruction. Conversely, dating in our temperature record at an annual resolution is assured from the cross-dating of 481 tree-ring series using standard dendrochronology methods (e.g. Fritts, 1976; Stokes and Smiley, 1968). Therefore, in order to obtain a similar offset than the one identified visually and to facilitate the comparison between the temperature and the TSI records, we used an accumulated linear adjustment for the TSI temporal scale deleting ~3 years per century before 757 AD, when the proxies to generate the TSI record changed (Figs. S4B and C).

We used the Multi-Taper Method (MTM; (Lees and Park, 1995)) to explore and identify significant cycles in our temperature and in the TSI records using the SSA-MTM toolkit (Ghil, 1997). In addition, to allow a simultaneous representation of the dominant modes of variability in both records and their variations and significances through time, we developed a Continuous Wavelet Transform (Grinsted et al., 2004; Torrence and Compo, 1998).

2.7. Temperature forcings from interannual to interdecadal scales

In order to analyze the climatic forcings of our temperature record from interannual to interdecadal scales, we analyzed the correlations of our reconstruction with a gridded ($2^\circ \times 2^\circ$) summer (December–March) reconstructed sea surface temperature (SST) across the Pacific (Huang et al., 2015) and with various temperature reconstructions from coral records in the tropical Pacific Ocean since *c.* 1600. This analysis considered the reconstructed (SST) in the western tropical Pacific Ocean with a monthly resolution (Tierney et al., 2015), the Niño Warm Pool (NWP) and the Niño Cold Tongue (NCT) indices, both seasonal (Freund et al., 2019).

3. Results and discussion

3.1. Temperature reconstruction for the last five millennia

Using available and newly developed *Fitzroya* tree-ring records we produced eight ring-width chronologies from sites located between 41° 32′and 42° 20′S that range from 1238 to 4456 years in length. Median and maximum core length for the tree-ring series at each site was 558 to 1037 and 1112 to 2248 years, respectively (Fig. 1, Table 1). Based on their strong correlations, we combined the data from these eight sites to produce a regional, 5682-year long, ring-width chronology (3672BC – 2009AD) based on 481 radii from 401 trees (Tables 1 and S1). This composite tree-ring record is the longest in the Southern Hemisphere and has a strong common signal with EPS ≥0.85 over more than 4300 years from 2328BC to 2009AD (Briffa and Jones, 1990, Fig. 1).

The strongest relationship between tree-ring width and temperature was found for the adjusted composite tree-ring chronology (*i.e.*, after the removal of the CO_2 effect on tree-ring growth) and mean maximum temperature during the previous summer (December–March). The temperature record is the regional average of four meteorological stations over the 1959–2009 period ($r = -0.67$, $p < 0.001$, $n = 51$, Fig. 3B, Table S4). Consistently, a significant negative relationship was also found between tree-ring growth and mean summer temperature from Valdivia between 1852 and 1883 ($r = -0.57$, P 0.001, $n = 32$; Fig. 3A). A similar negative relationship between *Fitzroya* growth and temperature has been previously reported (Lara and Villalba, 1993; Villalba, 1990) and explained as the result of increased evapotranspiration related to increased vapor pressure deficits during warm summers that negatively influence *Fitzroya* radial growth (Lara and Villalba, 1993; Urrutia-Jalabert et al., 2015a).

The reconstruction explains 49% of the total variance in the mean maximum summer temperature during the 51-year calibration period (1959–2009). The temporal stability and robustness of the reconstruction is indicated by the positive reduction of error statistic (RE = 0.46) and a Durbin-Watson statistic DW = 2.11, indicating that the residuals are not autocorrelated and have no significant trend over the 1959–2009 period (*slope* = 0.003, not

significant, Fig. 3C). This indicates the suitability of the adjusted chronology to reproduce the observed temperatures for the 1959–2009 period. Conversely, the reconstruction using the non-adjusted chronology fails to reproduce the observed temperatures, since it has a negative trend while the observed record has a significantly ($p < 0.01$) positive tendency (Fig. 4A). Moreover, the non-adjusted reconstruction estimates are in general above the instrumental record before *c.* 1975 and below this record after *c.* 1995 (Fig. 4A). This determines a significant slope ($p < 0.05$) and autocorrelation of the residuals (Fig. 4B, Table 2). Therefore, the removal of the CO_2 effect from the tree-ring chronology supported by the evidences provided in the methods section was necessary because otherwise there would be an underestimate of the observed temperatures since 1860. The adjustment is also important to produce a robust reconstruction as indicated by its statistics that fulfill the dendrochronology standards, which is not the case for the non-adjusted reconstruction (Table 2).

The adjustment to remove the effect of the CO_2 does not modify the sign and magnitude of the reconstructed temperature departures nor the temporal patterns regarding cycles and trends prior to AD 1860 when the adjusted and non-adjusted chronologies become identical (Fig. 2).

3.2. Temperature variations within a multi-millennial context

The summer temperature reconstruction presented in this study for the last 5680 years shows a positive slope over the entire period of the reconstruction ($p < 0.01$), consistent with an increase in summer solar insolation intensity over the Holocene in the SH (Fig. 3D; Porter, 1981). Orbital forcing has resulted in an increase in summer solar radiation over the Holocene in the SH contrasting with a decrease in the NH (Porter, 1981). This positive summer temperature trend is consistent with the pattern of larger, more extensive glacier advances in the mid-Holocene than during recent centuries in SSA, whereas maximum Holocene glacier advances in the NH occurred during the Little Ice Age interval or period (Kaplan et al., 2016; Mercer, 1968; Porter, 1981).

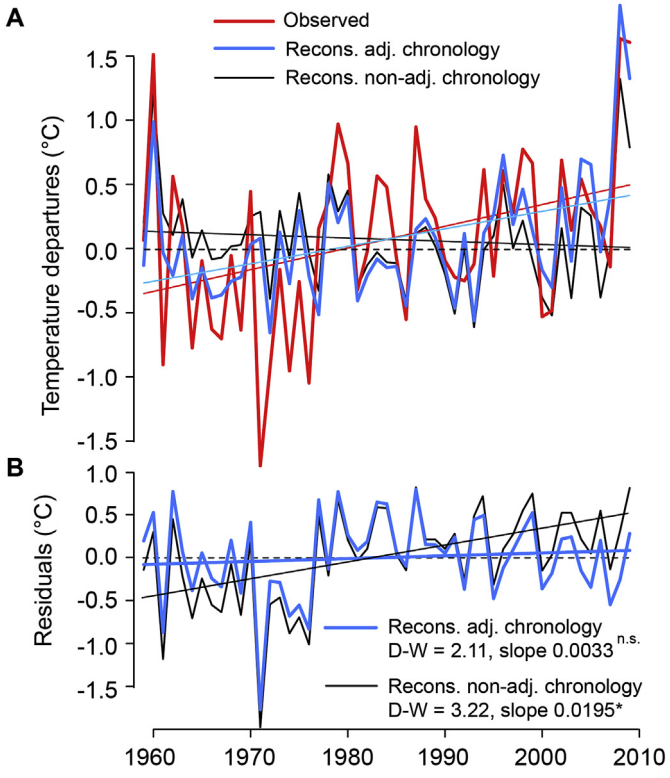

Fig. 4. (A) Mean maximum summer temperature departures (December–March) for the 1959–2009 period for observed records, reconstructed departures using the adjusted tree-ring chronology accounting for the removal of the increase in atmospheric CO_2 effect, and reconstructed departures using the non-adjusted chronology showing their respective linear trends; (B) Residuals of the reconstruction from the adjusted and unadjusted chronologies, indicating the Durbin-Watson (DW) statistic and slope indicated as n.s. (non-significant) or * ($p < 0.05$).

Table 2
Comparison between the regression models used for the reconstruction of mean maximum summer temperature departures (December–March) using non-adjusted versus adjusted *Fitzroya* chronologies for the removal of the effect of the increase in CO_2 concentration. Statistics defined in Fig. 3 caption.

Statistic	Non-adjusted chronology	Adjusted chronology
Correlation r	−0.56	−0.67
R^2_{adj}	0.31	0.49
F-value (1,49)	22.61	47.07
D-W	3.22	2.11

The most outstanding features in the reconstruction presented here are two major warm periods between 3140–2800 BC and 70 BC – 150 AD (5159–4819 and 2089–1869 years ago, respectively, counted from 2019 to facilitate comparisons with glacier records based on ^{10}Be dated moraines). During these warm periods, no glacier advances have been reported for Patagonia (Aniya, 2013; Kaplan et al., 2016; Strelin et al., 2014, Fig. 5A).

Our temperature record shows that the main periods of below average temperatures are: 3250–3140 BC, 2800–2670 BC, 2530–2360 BC, and 290–70 BC (Figs. 2D and 3A). These cold periods are, respectively, 5269–5159; 4819–4689; 4549–4379 and 2309-2089 years ago. The first three overlap in timing with the largest glacier expansions reported for southern Patagonia based on a ^{10}Be-dated chronology from Holocene moraines (Kaplan et al., 2016), and the 290–70 BC cold period is consistent with the latter portion of glacier expansion (Strelin et al., 2014, Fig. 5A). Aniya (1995) identified a glacier advance *ca.* 3600 BP (Neoglacial II in southern Patagonia), which is not consistent with a cold interval in the SSA temperature reconstruction (Fig. 5A). In contrast, the positive temperature departures in SSA around 3600 BC coincides with the absence of reported glacier advances (Kaplan et al., 2016) and the recorded dry-warm period based in pollen records from southern Patagonia (Moreno et al., 2018). Overall, the close agreement between the cold and warm periods in the early part of the reconstruction (i.e. before 2500 BC) and the independent glacier record (Kaplan et al., 2016) indicates the reliability of our temperature record despite the low number of tree-ring series in the early portion of this record (Figs. 1 and 5A).

In the last 2000 years, cold periods are less prominent and shorter compared to the earlier part of the reconstruction (Fig. 5A). The last four cold periods identified for AD 150–310, 655–730, 1180–1350 and 1530–1670 are concurrent with glacier advances reported by Strelin et al. (2014), and partially coincide with Kaplan et al. (2016, Fig. 5A). The 1530–1670 AD interval is also contemporaneous with Little Ice Age intervals or cold periods reported from a *Fitzroya* tree-ring record in Argentina and from dated moraines in the Argentinean and Chilean Patagonia between 40° to 55° S (Masiokas et al., 2009; Villalba, 1990). Despite the general agreement between our temperature reconstruction and glacier records, it should be noted that the timing of moraine building may slightly lag cold intervals. Also, shorter and less intense cold intervals may not be well represented in the moraine records because subsequently longer cold periods may erase the moraines formed by smaller glacier advances.

Reconstructed mean maximum temperature in our record

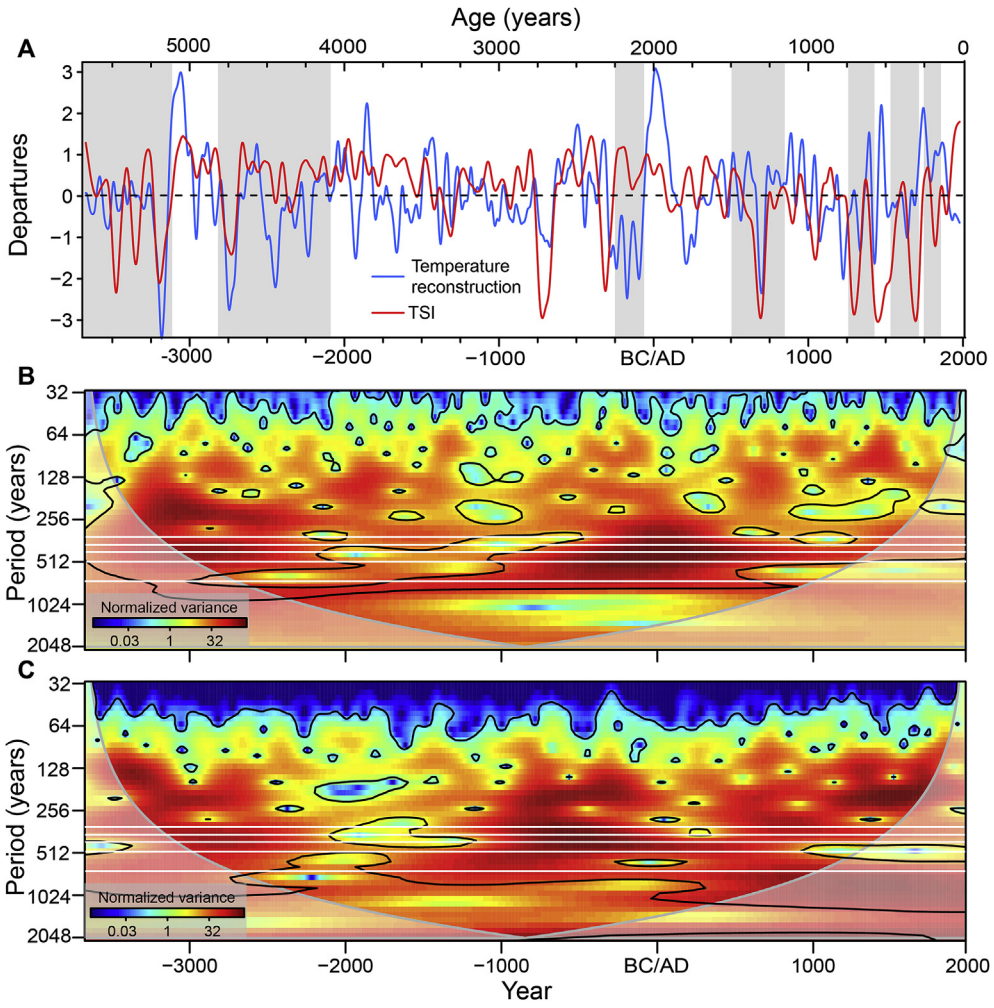

Fig. 5. (A) Comparison between the mean maximum temperature reconstruction (this study) and the Total Solar Irradiance (TSI) reconstruction (Steinhilber et al., 2012), indicating the main periods of glacier advance (Aniya, 2013; Kaplan et al., 2016; Strelin et al., 2014) as grey shaded rectangles; (B) Power amplitude spectrum of the Continuous Wavelet Transform indicating temporal cycles in the temperature reconstruction; (C) same for the TSI reconstruction. The thick black contours above the cone of influence designate the 95% confidence level against red noise. Horizontal white lines in the wavelets indicate the coincident long-term cycles between both records at 293, 372, 432–434, 512 and 746 years. Temperature and TSI records in all panels cover the period 3672 BC – 1977 AD (5650 years) and have been filtered with a 64-year spline to emphasize the low-frequency variability in both records. On top, age (years) counted from 2019 to facilitate comparisons with ^{10}Be dated moraines for glacier records (e.g. Kaplan et al., 2016; Strelin et al., 2014). (For interpretation of the references to colour in this figure legend, the reader is referred to the Web version of this article.)

shows warmer conditions during the 19th century (1780–1880 AD) than in the 20th century (Fig. 3D and Figs. 3D and S3). This pattern coincides with above average spring-summer temperatures during the 19th century, reconstructed from a completely independent 600-year record based on varved sediments from El Plomo Lake, Patagonia at 47° S (Elbert et al., 2015; Fig. S3, $r = 0.22$, $p < 0.001$, for the period 1780–2009). This is the warmest period in the entire El Plomo record (Elbert et al., 2015). Particularly warm summer conditions in the 1800s were also reported for Laguna Escondida in western Patagonia at ~45° S (Elbert et al., 2013) and for northern Argentinean Patagonia (Villalba, 1990). The 1775–1804 period has also been described as the warmest 30-year period in a millennial reconstruction for South America, south of 20° S (Neukom et al., 2011). Following the most important glacier advances in the 1600s related to the Little Ice Age interval, very few glacier advances have been registered during the 18th century (Luckman and Villalba, 2001; Masiokas et al., 2009; Ruiz et al., 2012).

In our study, recent decades (1959–2009) show a significant positive trend in both the observed and reconstructed mean maximum summer temperature records (Fig. 3B, *slope* = 0.017 and 0.014, $p = 0.008$ and 0.002, respectively). Nevertheless, this period, as well as the 20th century is not anomalously warm in the context of the last five millennia in the Pacific domain of southern South America (Fig. 3D). The two most noticeable warm periods in the reconstruction are actually higher in magnitude and duration than the positive temperature deviations during recent decades.

The subdued warming pattern during recent decades in our record is consistent with reports from instrumental records for southern Chile (38°–48°S), where there are no clear temperature patterns or significant trends reported over the period 1979–2009 (Falvey and Garreaud, 2009). Moreover, between 17° and 37° S, there is a clear contrast between surface cooling in coastal instrumental records and warming further inland in the Andes during the interval 1979–2009 (Falvey and Garreaud, 2009).

The temperature patterns in our reconstruction since 1950 are similar to those recorded in a recent reconstruction for the last 200 years, based on a δ^{13}C chronology from *Fitzroya* tree-rings for two sites located on the eastern slope of the Andes in Argentina (ca. 41° S; Lavergne et al., 2018). The clearest common pattern, the warming trend since the 1970s in both records, is also shown for north

Patagonia (i.e. 40° - 42° S; Villalba et al., 2003). However, Lavergne et al. (2018), and Villalba et al. (2003) describe warmer summer temperatures for the 20th century than during the 19th century, whereas our record shows the opposite pattern (Fig. 3D and Fig. S3). It has been previously documented that temperature variations may not be uniform between opposite slopes of the Patagonian Andes (40° - 42° S), since the western slope is more affected by the Pacific Ocean than the eastern slope (Villalba et al., 2003).

3.3. Temperature forcings at multi centennial scales

Visual comparison between our SSA temperature reconstruction and the adjusted TSI record (Steinhilber et al., 2012) indicate several coincidences between negative departures in solar irradiance and low reconstructed temperatures centered at 3195, 2730, 720 BC, and 695AD (5214, 4749, 2739, 1324 years ago, respectively, Fig. 5A). All these negative anomalies agree with cold intervals related to glacier advances in SSA (Kaplan et al., 2016; Strelin et al., 2014), except for the interval centered at 720 BC (Fig. 5A). Despite these agreements, the TSI record shows several negative anomalies that are not present in the reconstructed temperatures (i.e those centered at 3469 BC, 3340 BC, 310 BC and 1315 AD, and others after 750 AD, Fig. 5A). The Pearson correlation between our temperature reconstruction and the TSI record, both records filtered with a 64-year cubic spline, is $r = 0.22$, which despite being low, indicates a pattern of common variability that is consistent with the visual comparisons (Fig. S4A).

Consistent with the patterns documented in this paper, low frequency reconstructed cold temperature anomalies for the NH and periods of minimal solar activity were variable with periods of coincidences and discrepancies during the last 1200 years (Anchukaitis et al., 2017). Changes in large scale NH circulation are thought to provide a possible mechanism for these differences (Anchukaitis et al., 2017). The two major periods with positive anomalies in our reconstruction (3140–2800 BC and 70 BC-150 AD), coincide with positive anomalies of solar irradiance, but the deviations in the TSI are proportionally smaller in the latter period (Fig. 5A).

Multi-taper spectral analysis (Lees and Park, 1995) show remarkable coincidences between the long-term cycles in our temperature record and the TSI reconstructions at 293, 372, 432–434, 512 and 746 years, all significant at $p < 0.05$ (Fig. 6).

The significant cycles in the adjusted TSI record are almost the same as those recorded in the non-adjusted TSI record, as an indication that the spectral structure remains unaltered after the linear adjustment (Fig. S5). Some of these cycles are very close to those reported for the TSI record at 350, 500 and 710 years (Steinhilber et al., 2012). Consistently, continuous wavelet transform indicates high normalized variance in the range of the cycles shown by the Multi-taper spectral analysis both for the temperature and the TSI records during an important portion of the period above the cone of influence (Fig. 5B and C and 6A and B). Nevertheless, the temporal patterns are not stationary and show differences in strength through time (Fig. 5B and C). A similar pattern of non-stationary character through time has been described for the dominant 208-year De Vries' (or Suess) solar cycle (Anchukaitis et al., 2017).

3.4. Temperature forcings from interannual to interdecadal scales

Spatial correlation patterns show a clear association between instrumental and reconstructed temperature records and summer sea surface temperatures (SST) across the Pacific off the South American coast (Huang et al., 2015). Significant correlations were recorded during the period 1959–2009, as well as for the total

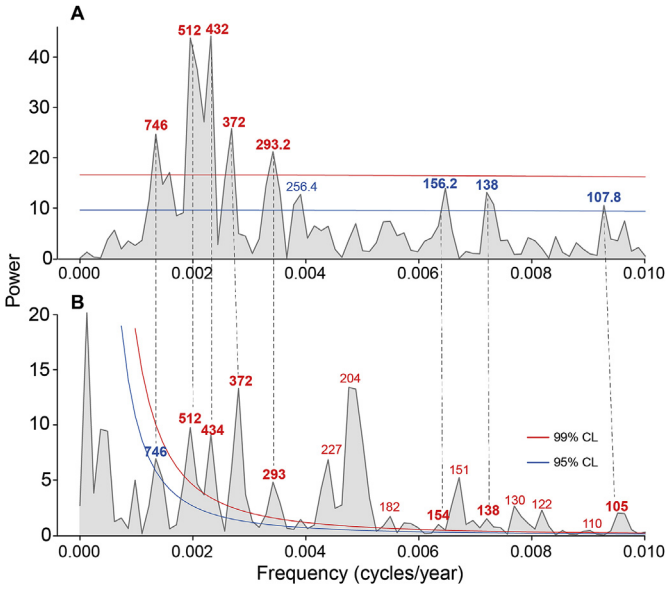

Fig. 6. (A) Significant cycles identified by the Multi-Taper Method (MTM, Lees and Park, 1995) for the temperature reconstruction and (B) same for the TSI record showing the spectrum for cycles ≥ 100 years. Numbers in blue and red indicate the cycles (in years) that are significant at 95% and 99%, respectively. (For interpretation of the references to colour in this figure legend, the reader is referred to the Web version of this article.)

overlapping period between the two records (1855–2009, $p < 0.05$, Fig. 7). These correlation fields are consistent with previous studies that document the influence of the variations in the Pacific Ocean circulation over the climate in northwestern Patagonia (Garreaud et al., 2009; Montecinos and Aceituno, 2003).

The occurrence of warm (El Niño) events of the Southern Oscillation (SO) is associated with warmer and drier summers in the Andes between 38° and 41° S (Montecinos and Aceituno, 2003). Similarly, the change from the negative to the positive phase in the Pacific Decadal Oscillation (PDO) in 1976/77 has been associated with an abrupt increase in temperature along the Pacific Coast of South America, especially in summer (December–March, Villalba et al., 2003; Vuille et al., 2015).

The SSA summer temperature reconstruction presented in this study is related to the summer-fall (December–May) Niño Cold Tongue (NCT) for the 1617–2007 common period ($r = 0.16$, $n = 361$, $p < 0.01$). This seasonal index was constructed from a network of 27 coral records and is associated with sea surface temperature (SST) in the eastern equatorial Pacific that expands towards the South America coasts (Freund et al., 2019). The patterns of our temperature record were more related to those of the NCT index than with the SST reconstruction (Tierney et al., 2015) or the NWP (Freund et al., 2019). Therefore we selected the NCT index for further analysis.

Our summer temperature record has common coherent variations with the NCT as a SST proxy, from interannual to interdecadal scales for the last 391 years (Fig. 8). Both records are highly coherent particularly at cycles of 2.6–2.8, 3.0–3.1 and 4.6 years, and also at 40 through 80 and up to 100 years, indicating a high persistence of temperature patterns in the Pacific (Fig. 8C). At an interdecadal scale, both records show common oscillations in the 15–20 and 25-30-year range, particularly in the 1617–1800 period (Fig. 8B). Nevertheless, both records have opposite trends after the 1980s. The variations estimated through first differences indicate the occurrence of marked interannual temperature changes in both records mostly associated with ENSO warm and cold events

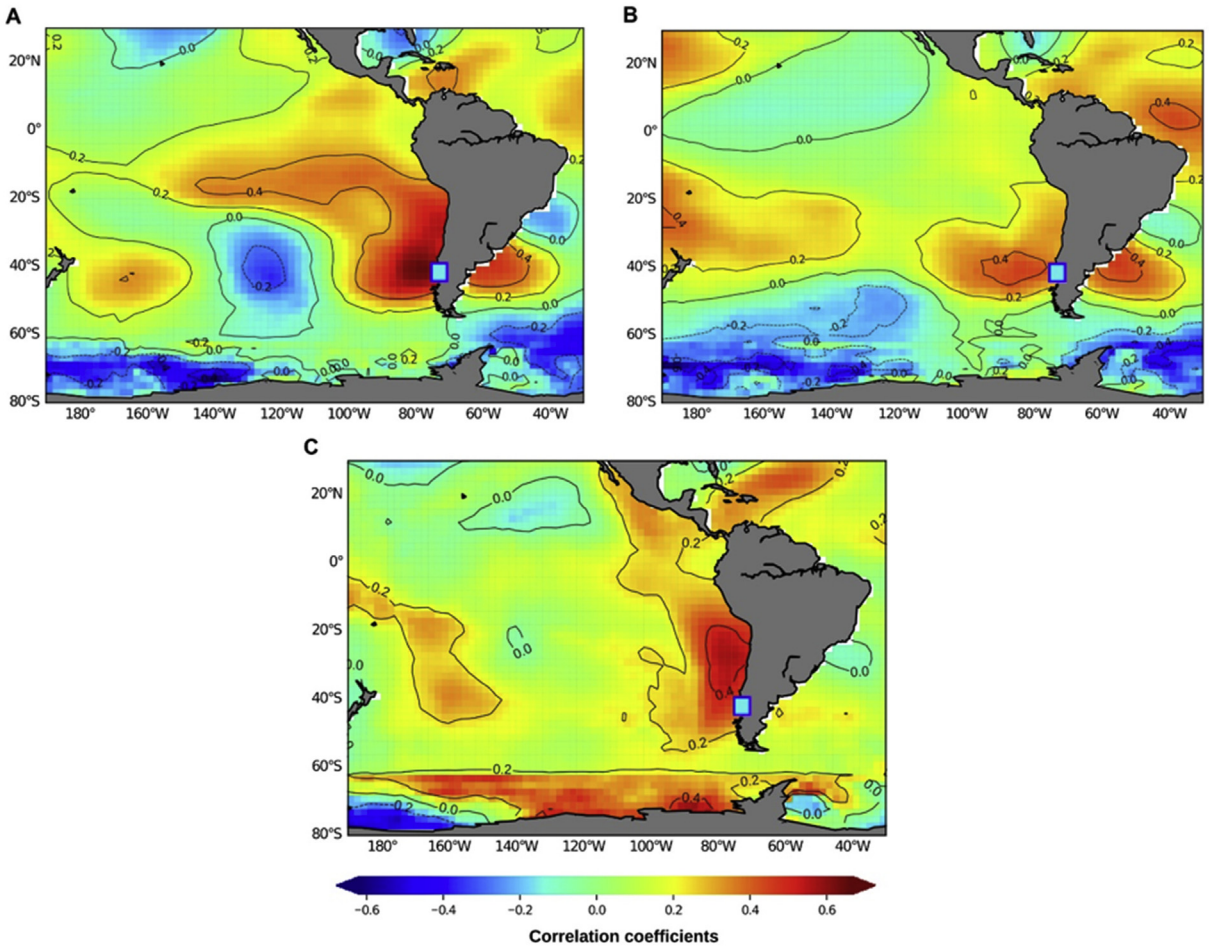

Fig. 7. Spatial correlation patterns between December–March (summer) sea surface temperatures from Huang et al. (2015) and: (A) observed December–March regional mean maximum temperature from the meteorological stations identified in Table S2 for the period 1959–2009; (B) reconstructed December–March mean maximum temperature for the period 1959–2009, and (C) same as *B* for the period 1855–2009. Critical Pearson correlation significant at 95% for the 1959–2009 interval is $r = \pm 0.257$.

(Fig. 8D). There are many warm (El Niño) and cold (La Niña) ENSO events defined by Quinn and Neal (1992) and Ortlieb (2000) that match above and below average summer temperatures in our southern South America temperature record and SST in the eastern tropical Pacific (Fig. 8D). However, not all the ENSO warm events reported by Quinn and Neal (1992) and Ortlieb (2000) for the last four centuries are captured in any or both reconstructions. Interestingly, the relationships between the SSA temperature and the NCT Sea Surface Temperatures over the tropical Pacific based on moving segments of 30 years on the first-differences (Fig. 8D and E) are quite variable, with alternating 50-75 year-cycles with correlation coefficients (r) between 0.5 and 0.6 and then falling to $r = 0$ or even negative (Fig. 8E). This is a clear indication of the instability in the relationship between ENSO and SSA temperature, likely modulated by interactions with other internal climatic forcings such as SAM and the PDO.

We selected some extreme ENSO events from the SST instrumental period to analyze the spatial patterns of the relationship between our temperature reconstruction and observed SST (Fig. 8F). The 1919 positive anomaly in our reconstruction is consistent with the spatial pattern of above average summer-fall (December–May) NCT over a large area throughout the eastern tropical Pacific and reaching the South American coasts. This influence is particularly strong at the Equator and over a wide latitudinal range reaching 35° S (based on HADLSST1 records; Rayner et al., 2003, Fig. 8F). The 1877 warm ENSO event has been considered as the most severe for the 19th century. Our summer (December–March) temperature reconstruction recorded this year was an outstanding positive anomaly, but is not a relevant departure in the NCT record (Fig. 8F). The differences between both records for the summer of 1877 are highly consistent with the spatial patterns of HADLSST1 (Rayner et al., 2003) that indicate that the warm SST anomalies were clearly more intense off the Chilean Coast than in eastern tropical Pacific (Fig. 8F). This anomaly extended across the coasts of Perú and Chile reaching (40° S). The opposite cold (La Niña) ENSO events in 1974 and 1921 were also recorded in both temperature reconstructions as negative anomalies. This is consistent with the spatial patterns of the HADLSST1 SST indicating below mean temperatures from the tropical Pacific to the coasts of SSA (Fig. 8F). The 1921 cold event covers a wider latitudinal range off the western coast of South America including Patagonia (17° - 55° S, Fig. 8F).

Other studies have documented the relevance of other drivers of interannual to interdecadal climatic variability in southern South America during the 20th century, including the Southern Annual Mode (SAM, Garreaud et al., 2009; Gillett et al., 2006; Villalba et al., 2012), and the latitudinal position and intensity of the Permanent Pacific Anticyclone (Barrett and Hameed, 2017; Pittock, 1980).

A detailed analysis of the influence of these internal climatic drivers in our record is beyond the scope of this paper.

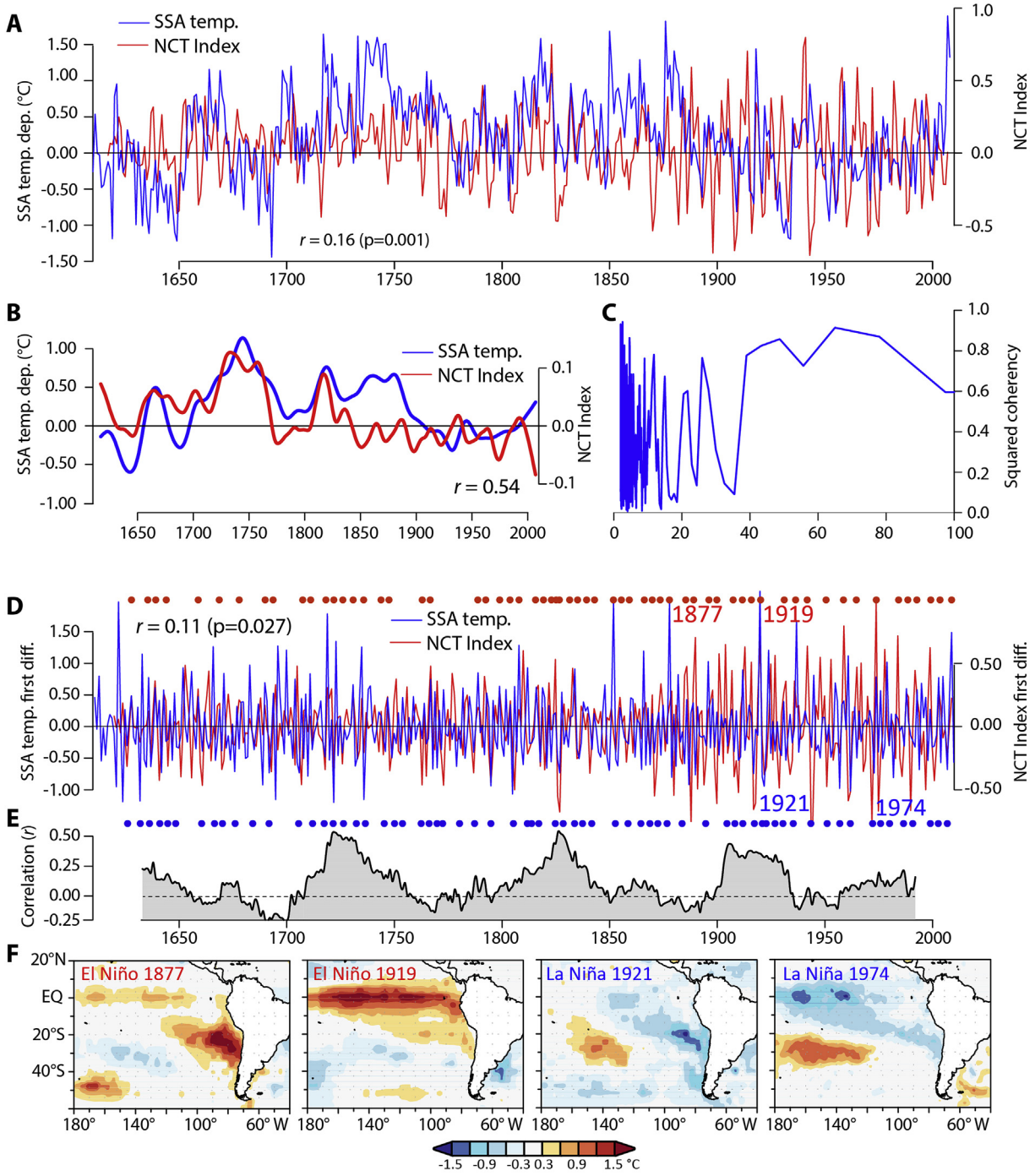

Fig. 8. (A). Mean maximum temperature reconstruction for southern South America (SSA, this study) and the summer-fall (December–May) seasonal Niño Cold Tongue (NCT) index for the period 1617–2007 (N = 391) developed from a network of seasonally resolved coral records (Freund et al., 2019); (B) Same records filtered to analyze their decadal and interdecadal patterns of variation; (C) Squared coherency of both records indicating their common temporal patterns; (D) First differences of each record to emphasize years with positive (red dots) and negative (blue dots) departures in both SSA temperature and NCT record. (E) Correlations between SSA and NCT first-differences for 30 year-moving segments lagged one year (F) SST (December to March) anomalies in the Pacific Ocean off the South American coast for El Niño 1877, 1919 events and La Niña 1921, 1974 events, SST from HADLSST1 records (Rayner et al., 2003). (For interpretation of the references to colour in this figure legend, the reader is referred to the Web version of this article.)

Nevertheless, results presented here are an indication that our multi-millennial temperature reconstruction offers a unique opportunity for the documentation of the complex relationships between global and hemispheric climatic drivers acting on different temporal scales that modulate climate variability in southern South America.

4. Conclusions

The new 5682-year tree-ring mean maximum summer temperature (December–March) record for southern South America (SSA) presented here is the longest such annually resolved record for the Southern Hemisphere. Our record explains 49% of the mean maximum summer temperature variation for the 1959–2009

calibration period and covers the second half of the Holocene. This record expands the length of available annually resolved climate reconstructions from any continuous proxy in the Southern Hemisphere by 2062 years in South America, 2072 additional years in the case of Tasmania and 4572 years for New Zealand (Cook et al., 2006; Lara and Villalba, 1993).

The development of an innovative method for the removal of the effect of higher atmospheric CO_2 concentration on increased tree-ring growth reported for *Fitzroya* in Chile and Argentina (Lavergne et al., 2018; Urrutia-Jalabert et al., 2015a) was necessary for producing the temperature reconstruction. This method included the development of an adjusted tree-ring chronology using regression techniques that conforms to observed temperature trends in recent decades and provides robust statistical models. The need to remove the effects of CO_2 fertilization on tree ring data before calibrating climate reconstruction models is a necessary requirement to avoid biased results (Scharnweber et al., 2019).

Our annually resolved temperature reconstruction for SSA retains low frequency variability, documenting centennial and multicentennial temperature anomalies with a slight positive trend throughout the last 5680 years. The most outstanding features in the temperature record are two major warm periods between 3140–2800 BC and 70 BC – 150 AD (5159–4819 and 2089–1869 years prior to 2019). During these warm periods, no glacier advances have been identified in SSA (Aniya, 2013; Kaplan et al., 2016; Strelin et al., 2014). Our temperature record shows that the main century-long periods of below average temperatures are: 3250–3140 BC, 2800–2670 BC, 2530–2360 BC, and 290–70 BC, which coincide with glacier expansions reported for Patagonia (Kaplan et al., 2016; Strelin et al., 2014). These cold periods occurred at: 5269–5159; 4819–4689; 4549–4379; and 2309-2089 years ago from 2019, respectively. In recent centuries reconstructed mean maximum temperature in our record shows warmer conditions during the 19th century (1780–1880 AD) than in the 20th century. Interestingly this pattern coincides with the one shown by a completely independent 600-year spring-summer temperature record based on varved sediments from El Plomo Lake, Patagonia 47° S (Elbert et al., 2015).

The tree-ring summer temperature record presented here indicates a warming trend in southern South America since the 1960s. Nevertheless, this pattern is not unprecedented in the context of the last five millennia, during which several warm periods larger in magnitude and duration are recorded. This pattern for the last decades is in agreement with recent trends reported in instrumental temperature records that suggest that the mid-latitudes of the ocean-dominated Southern Hemisphere are not warming at the same rate as other areas in the last four decades (Falvey and Garreaud, 2009).

Solar radiation is an important forcing of temperature variability at multi-centennial timescales for SSA for the last 5650 years. Although, this temperature driver has already been reported for the Northern Hemisphere, our study is the first to document its influence on temperature in the Southern Hemisphere for the last millennia. Coincidences occur between negative departures in an independent record of Total Solar Irradiance (TSI) and low temperatures in our reconstruction centered at 3195, 2730, 720 BC, and 695AD.

The strength of solar forcing in our temperature record is demonstrated by the coincidences between the long-term cycles in our temperature record and the TSI reconstructions at 293, 372, 432–434, 512 and 746 years, all significant at $p < 0.05$. Our 5682-year temperature reconstruction, based on tree-ring series up to 2200 years' length, was able to detect long cycles that cannot be found in shorter tree-ring records and reconstructions for the last two millennia or shorter.

At interannual to interdecadal scales, reconstructed summer temperature variations have been mainly related to the summer-fall (December–May) Niño Cold Tongue (NCT, Freund et al., 2019) a seasonal proxy of sea surface temperature developed from coral records for the 1617–2007 period. NCT is an expression of the internal climate variability in SSTs on the eastern equatorial Pacific which frequently expands towards the Southern South America coasts. Significant correlations between our reconstruction and gridded summer sea surface temperatures across a broad area of the Eastern Pacific off the South American coast since 1850 support the connections between summer temperatures in southern South America and Pacific Ocean SST variations. However, the influence of the Pacific Ocean on temperature variability in southern South America is complex due to the interactions of the various tropical forcings with extra-tropical climate modes of variability such as the Southern Annular Mode (SAM), generating specificities in regional to sub-continental temperature variations not observed at a global scale.

The new southern South America temperature reconstruction presented in this paper contributes to our understanding of climate variations at centennial or longer time scales over the past five millennia, for a poorly documented area in the Southern Hemisphere (Neukom et al., 2014). Our record also has an interannual and interdecadal signal. The absence of an unprecedented increase in temperature in recent decades in SSA shows that changes in radiative forcings (solar and anthropogenic) interact with internal modes of variability of the Pacific Ocean-atmosphere system.

Our study reveals the need to characterize regional-scale climate variability and its drivers, which in the context of global-scale processes such as anthropogenic warming, interact to modulate local climates affecting humans and ecosystems.

Data availability

All the datasets generated and/or analyzed during the current study will be available at https://www.cr2.cl/datos-dendro-clima/.

Acknowledgements

This work was supported by FONDECYT Grants N° 1130410 and 1171496, the Center for Climate and Resilience Research (CR)^2 funded by CONICYT/FONDAP/15110009, the IAI grant CRNII 2047b and BNP-PARIBAS Foundation. RV is supported by CONICET-Argentina, RUJ by the Fondecyt Postdoctoral Grant 3160258 and Project PAI CONICYT 7818I20003. JCA acknowledges support from FONDECYT Grant 1130381 and AG from Comisión Nacional de Investigación Científica y Tecnológica–Programa de Capital Humano Avanzado (CONICYT-PCHA)/Doctorado Nacional/2016-21160642) We thank the Chilean National Forest Service (CONAF), for their permission to work with *Fitzroya* trees within National Protected Areas and Ed Cook, for his support and commitment to adapt the RCSigFree tree-ring Standardization Program to run long tree-ring chronologies.

Appendix A. Supplementary data

Supplementary data to this article can be found online at https://doi.org/10.1016/j.quascirev.2019.106087.

References

Anchukaitis, K., DÁrrigo, R., Amndreu-Hayles, L., 2013. Tree-ring-reconstructed summer temperatures from northwestern north America during the last nine centuries. J. Clim. 26, 3001–3012.

Anchukaitis, K., Wilson, R., Briffa, K.R., Büntgen, U., Cook, E.R., Arrigo, R.D., Davi, N., Esper, J., Frank, D., Linderholm, H.W., Myglan, V., Osborn, T.J., Zhang, P., Rydval, M., Schneider, L., Schurer, A., Wiles, G., Zorita, E., 2017. Last millennium Northern Hemisphere summer temperatures from tree rings : Part II , spatially resolved reconstructions. Quat. Sci. Rev. 163, 1–22. https://doi.org/10.1016/j.quascirev.2017.02.020.

Aniya, M., 2013. Holocene glaciations of hielo patagónico (Patagonia icefield), South America: a brief review. Geochem. J. 47, 97–105.

Aniya, M., 1995. Holocene glacial chronology in Patagonia: Tyndall and Upsala glaciers. Artic Alp. Res. 27, 311–322.

Aravena, J.C., Lara, A., Wolodarsky-Franke, A., Villalba, R., Cuq, E., 2002. Tree-ring growth patterns and temperature reconstruction from Nothofagus pumilio (Fagaceae) forests at the upper tree line of southern Chilean Patagonia. Rev. Chil. Hist. Nat. 75, 361–376.

Barrett, B., Hameed, S., 2017. Seasonal variability in precipitation in central and southern Chile: modulation by the South Pacific high. J. Clim. 30, 55–69.

Berger, A., Loutre, M.F., 1991. Insolation values for the climate of the last 10 million years. Quat. Sci. Rev. 10, 297–317.

Breitenmoser, P., Beer, J., Brönnimann, S., Frank, D., Steinhilber, F., Wanner, H., 2012. Solar and volcanic fingerprints in tree-ring chronologies over the past 2000 years. Palaeogeogr. Palaeoclimatol. Palaeoecol. 313–314, 127–139. https://doi.org/10.1016/j.palaeo.2011.10.014.

Briffa, K.R., Jones, P., 1990. Basic Chronology Statistics and Assessment. Kluwer Academic Publishers.

Camarero, J.J., Gazol, A., Galván, J.D., Sangüesa-Barreda, G., Gutiérrez, E., 2015. Disparate effects of global-change drivers on mountain conifer forests: warming-induced growth enhancement in young trees vs. CO2 fertilization in old trees from wet sites. Glob. Chang. Biol. 21, 738–749. https://doi.org/10.1111/gcb.12787.

Christie, D., Bonisegna, J., Cleaveland, M., Lara, A., Le Quesne, C., Morales, M., Mudelsee, M., Stahle, D., Villalba, R., 2011. Aridity changes in the Temperate-Mediterranean transition of the Andes since AD 1346 reconstructed from tree-rings. Clim. Dyn. 36, 1505–1521. https://doi.org/10.1007/s00382-009-0723-4.

Cook, E., Briffa, K., Meko, D., Graybill, D., Funkhouser, G., 1995. The segment length curse in long tree-ring chronology development for palaeoclimatic studies. Holocene 5, 229–237.

Cook, E., Buckley, B., Palmer, J., Fenwick, P., Peterson, M., Boswijk, G., Fowler, A., 2006. Millennia-long tree-ring records from Tasmania and New Zealand: a basis for modelling climate variability and forcing, past, present and future. J. Quat. Sci. 21, 689–699.

Cook, E.R., 2017. RCSigFree, Software Specialized in Dendrochronology [WWW Document]. Columbia Univ. http://www.ldeo.columbia.edu/tree-ring-laboratory/resources/software/.

Elbert, J., Jacques-coper, M., Daele, M. Van, Urrutia, R., Grosjean, M., 2015. A 600 years warm-season temperature record from varved sediments. Quat. Int. 377, 28–37. https://doi.org/10.1016/j.quaint.2015.01.004.

Elbert, J., Wartenburger, R., von Gunten, L., Urrutia, R., Fischer, D., Fujak, M., Hamann, Y., David Greber, N., Grosjean, M., 2013. Late Holocene air temperature variability reconstructed from the sediments of Laguna Escondida, Patagonia, Chile (45°30′S). Palaeogeogr. Palaeoclimatol. Palaeoecol. 369, 482–592.

Falvey, M., Garreaud, R.D., 2009. Regional cooling in a warming world: recent temperature trends in the southeast Pacific and along the west coast of subtropical South America (1979-2006). J. Geophys. Res. 114, 1–16.

Frank, D.C., Poulter, B., Saurer, M., et al., 2015. Water-use efficiency and transpiration across European forests during the Anthropocene. Nat. Clim. Chang. 5, 579–583.

Freund, M., Henley, B., Karoly, D., McGregor, H., Abram, N., Dommenget, D., 2019. Higher frequency of Central Pacific El Niño events in recent decades relative to past centuries. Nat. Geosci. 12, 450–455.

Fritts, H., 1976. Tree Rings and Climate. Academic Press, London.

Garreaud, R.D., Vuille, M., Compagnucci, R., Marengo, J., 2009. Present-day south American climate. Palaeogeogr. Palaeoclimatol. Palaeoecol. 281, 180–195.

Ghil, M., 1997. The SSA-MTM toolkit: applications to analysis and prediction of time series. In: Proc. SPIE 3165, Applications of Soft Computing. San Diego.

Gillett, N., Kell, T., Jones, P., 2006. Regional climate impacts of the southern annular mode. Geophys. Res. Lett. 33.

Grinsted, A., Moore, J.C., Jevrejeva, S., 2004. Application of the cross wavelet transform and wavelet coherence to geophysical time series. Nonlinear Process. Geophys. 11, 561–566.

Guerrieri, R., Belmecheri, S., Ollinger, S., Asbjornsen, H., Jennings, K., Xiao, J., Stocker, B., Martin, M., Hollinger, D., Bracho-Garrillo, R., Clark, K., Dore, S., Kolb, T., Munger, W., Novick, K., Richardson, A., 2019. Disentangling the role of photosynthesis and stomatal conductance on rising forest water-use efficiency. Proc. Natl. Acad. Sci. 116, 16909–16914. https://doi.org/10.1073/pnas.1905912116.

Hartmann, D.L., Klein Tank, A., Rusticucci, M., Alexander, L., Brönnimann, S., Charabi, Y., Dentener, F., Dlugokencky, E., Easterling, D., Kaplan, A., Soden, B., Thorne, P., Wild, M., Zhai, P., 2013. Observations: atmosphere and surface. In: Stocker, T.F., Qin, D., GK, Plattner, M., Tignor, S.K., Allen, J., Boschung, A., Nauels, Y., Xia, V.B., PMM (Eds.), Climate Change 2013: the Physical Science Basis. Contribution of Working Group I to the Fifth Assessment Report of the Intergovernmental Panel on Climate Change. Cambridge University Press, Cambridge, United Kingdom and New York, NY, USA, pp. 159–254.

Hegerl, G., Crowley, T., Allen, M., Hyde, W.T., Pollack, H., Smerdon, J., Zorita, E., 2007. Detection of human influence on a new, validated 1500-year temperature reconstruction. J. Clim. 20, 650–666.

Hegerl, G., Crowley, T.J., Baum, S.K., Kim, K.Y., Hyde, W., 2003. Detection of volcanic, solar and greenhouse gas signals in paleo-reconstructions of Northern Hemispheric temperature. Geophys. Res. Lett. 30, 1–4.

Hegerl, G., Hasselmann, K., Cubash, U., Mitchell, J.F., Roeckner, E., Voss, R., Waszkewitz, J., 1997. Multi-fingerprint detection and attribution analysis of greenhouse gas, greenhouse gas-plus-aerosol and solar forced climate change. Clim. Dyn. 13, 613–634.

Holmes, R.L., 1983. Computer-assisted quality control in tree-ring dating and measurement. Tree-Ring Bull. 43, 69–78.

Huang, B., Banzon, V., Freeman, E., Lawrimore, J., Liu, W., Peterson, T.C., Smith, T., Thorne, P.W., Woodruff, S.D., Zhang, H., 2015. Extended reconstructed sea surface temperatures version 4 (ERSST.v4), Part I. upgrades and intercomparisons. J. Clim. 28, 911–930.

Huang, R., Zhu, H., Liu, X., Liang, E., Briebinger, J., Wu, G., Li, X., Bräuning, A., 2017. Does increasing intrinsic water use efficiency (iWUE) stimulate tree growth at natural alpine timberline on the southeastern Tibetan Plateau? Glob. Planet. Change 148, 217–226.

Kaplan, M.R., Schaefer, J.M., Strelin, J.A., Denton, G.H., Anderson, R.F., J, V.M., Finkel, R.C., Schwartz, R., Travis, S.G., García, J.L., Martini, M.A., Nielsen, S.H.H., 2016. Patagonian and Southern South Atlantic view of Holocene climate. Quat. Sci. Rev. 141, 112–125.

Keenan, T.F., Hollinger, D.Y., Bohrer, G., Dragoni, D., Munger, J.W., Schmid, H.P., Richardson, A.D., 2013. Increase in forest water-use efficiency as atmospheric carbon dioxide concentrations rise. Nature 499, 324–327. https://doi.org/10.1038/nature12291.

Koutavas, A., 2013. CO2 fertilization and enhanced drought resistance in Greek firs from Cephalonia Island, Greece. Glob. Chang. Biol. 19, 529–539. https://doi.org/10.1111/gcb.12053.

Lara, A., Bahamondez, A., González-Reyes, A., Muñoz, A., Cuq, E., Ruiz-Gomez, C., 2015. Reconstructing streamflow variation of the Baker river from tree-rings in northern Patagonia since 1765. J. Hydrol. 529, 511–523.

Lara, A., Villalba, R., 1993. A 3620-year temperature record from Fitzroya cupressoides tree rings in southern South America. Science (80-.) 260, 1104–1106.

Lara, A., Villalba, R., Aravena, J.C., Wolodarsky-Franke, A., Neira, E., Roig, F., 2000. Desarrollo de una red de cronologias de Fitzroya cupressoides (Alerce) para Chile y Argentina. In: Dendrocronologia En America Latina. EDIUNC, Mendoza, Argentina, pp. 217–244.

Lara, A., Villalba, R., Urrutia, R., 2008. A 400-year tree-ring record of the Puelo River summer-fall streamflow in the Valdivian Rainforest eco-region, Chile. Clim. Change 86, 331–356.

Lavergne, A., Daux, V., Pierre, M., Stievenard, M., Srur, A.M., Villalba, R., 2018. Past summer temperatures inferred from dendrochronological records of Fitzroya cupressoides on the eastern slope of the northern Patagonian Andes. J. Geophys. Res. G Biogeosci. 123, 32–45. https://doi.org/10.1002/2017JG003989.

Lees, J.M., Park, J., 1995. Multiple-taper spectral analysis: a stand-alone C-subroutine. Comput. Geosci. 21, 199–236.

Lévesque, M., Siegwolf, R., Saurer, M., Eilmann, B., Rigling, A., 2014. Increased water-use efficiency does not lead to enhanced tree growth under xeric and mesic conditions. New Phytol. 203, 94–109. https://doi.org/10.1111/nph.12772.

Luckman, B., Villalba, R., 2001. Assessing the synchroneity of glacier fluctuations in the western cordillera of the Americas during the last millennium. In: Markgraf, V. (Ed.), Nterhemispheric Climate Linkages. Academic Press, London, pp. 119–140.

Martínez-Vilalta, J., López, B.C., Adell, N., Badiella, L., Ninyerola, M., 2008. Twentieth century increase of Scots pine radial growth in NE Spain shows strong climate interactions. Glob. Chang. Biol. 14, 2868–2881. https://doi.org/10.1111/j.1365-2486.2008.01685.x.

Masiokas, M., Rivera, A., Espizua, L., Villalba, R., Delgado, S., Aravena, J.C., 2009. Glacier fluctuations in extratropical South America during the past 1000 years. Palaeogeogr. Palaeoclimatol. Palaeoecol. 281, 242–268.

Masson-Delmotte, V., Schulz, M., Abe-Ouchi, A., Beer, J., Ganopolski, A., González Rouco, J.F., Janse, E., Lambeck, K., Luterbacher, J., Naish, T., Osborn, T., Otoo-Bliesner, B., Quinn, T., Ramesh, R., Rojas, M., Shao, X., Timmermann, A., 2013. Information from Paleoclimate archives. In: Stocker, T.F., Qin, D., Plattner, G.K., Tignor, M., Allen, S.K., Boschung, J., Nauels, A., Xia, Y., Bex, V., Midgley, P.M. (Eds.), Climate Change 2013: the Physical Science Basis. Contribution of Working Group I to the Fifth Assessment Report of the Intergovernmental Panel on Climate Change. Cambridge University Press, Cambridge, Cambridge.

Meko, D., 1997. Dendroclimatic reconstruction with time varying subsets of tree indices. J. Clim. 10, 687–696.

Melvin, T.M., Briffa, K.R., 2008. A “signal-free” approach to dendroclimatic standardisation. Dendrochronologia 26, 71–86.

Mercer, J., 1968. Variations of some Patagonian glaciers since the late glacial. Am. J. Sci. 266, 91–109.

Michaelsen, J., 1987. Cross-validation in statistical climate forecast models. J. Appl. Meteorol. Climatol. 26, 1589–1600.

Montecinos, A., Aceituno, P., 2003. Seasonality of the ENSO related rainfall variability in central Chile and associated circulation anomalies. J. Clim. 16, 281–296.

Moreno, P., Vilanova, I., Villa-Martinez, R., Dunbar, R., Mucciarone, D., Kaplan, M., Garreaud, R., Rojas, M., Moy, C., De Pol-Holz, R., Lambert, F., 2018. Onset and evolution of southern Annular mode-like changes at centennial timescale. Sci. Rep. 8, 1–9.

Muñoz, A.A., González-Reyes, A., Lara, A., Sauchyn, D., Christie, D., Puchi, P., Urrutia-Jalabert, R., Toledo-Guerreo, I., Aguilera-Betti, I., Mundo, I., Sheppard, P.R., Stahle, D., Villalba, R., Szejner, P., Le Quesne, C., Vanstone, J., 2016. Streamflow variability in the Chilean Temperate-Mediterranean climate transition (35°S–42°S) during the last 400 years inferred from tree-ring records. Clim. Dyn. 47, 4051–4066.

Neukom, R., Gergis, J., Karoly, D.J., Wanner, H., Curran, M., Elbert, J., González-rouco, F., Linsley, B.K., Moy, A.D., Mundo, I., Raible, C.C., Steig, E.J., Ommen, T. Van, Vance, T., Villalba, R., Zinke, J., Frank, D., 2014. Inter-hemispheric temperature variability over the past millennium. Nat. Clim. Chang. 4, 362–367. https://doi.org/10.1038/NCLIMATE2174.

Neukom, R., Luterbacher, J., Villalba, R., Kuttel, M., Frank, D., Jones, P.D., Grosjean, M., Wanner, H., Aravena, J.C., Black, D.E., Christie, D., D'Arrigo, R., Lara, A., Morales, M., Soliz-Gamboa, C., Srur, A., Urrutia, R., von Gunten, L., 2011. Multiproxy summer and winter surface air temperature field reconstructions for southern South America covering the past centuries. Clim. Dyn. 37, 35–51. https://doi.org/10.1007/s00382-010-0793-3.

Ortlieb, L., 2000. The documentary historical record of El Niño events in Peru: an update of the Quinn record (sixteenth through nineteenth centuries). In: Diaz, H., Markgraf, V. (Eds.), El Niño and the Southern Oscillation: Variability, Global and Regional Impacts. Cambridge University Press, Cambridge, pp. 207–295.

Ostrom, C.W., 1990. Time Series Analysis: Regression Techniques, second ed. Sage University Paper.

Pages 2k Consortium, 2013. Continental-scale temperature variability during the past two millennia. Nat. Geosci. 6, 339–345. https://doi.org/10.1038/NGEO1797.

Pittock, A., 1980. Patterns of climate variation in Argentina and Chile - I. precipitation, 1931–1960. Mon. Weather Rev. 108, 1362–1369.

Porter, S.C., 1981. Glaciological evidence of Holocene climatic change. In: Wigley, T.M., Ingram, M.J., Farmer, G. (Eds.), Climate and History Studies on Past Climates and Their Impact on Man. Cambridge University Press, Cambridge, pp. 82–110.

Quinn, W., Neal, V., 1992. The historical record of El Niño events. In: Bradley, R., Jones, P. (Eds.), Climate since A.D. 1500. Routledge, London, pp. 623–648.

Rayner, N., Parker, D., Horton, E., Folland, C., Alexander, L., Rowell, D., Kent, E., Kaplan, A., 2003. Global analyses of sea surface temperature, sea ice, and night marine air temperature since the late nineteenth century. J. Geophys. Res. 108 (D14).

Roig, F., Le Quesne, C., Boninsegna, J.A., Briffa, K., Lara, A., Grudd, H., Jones, P.D., Villagrán, C., 2001. Climate variability 50,000 years ago in mid-latitude Chile as reconstructed from tree rings. Nature 410, 567–570.

Ruiz, L., Masiokas, M., Villalba, R., 2012. Fluctuations of glaciar Esperanza Norte in the North Patagonian Andes of Argentina during the past 400 yr. Clim. Past 8, 1079–1090.

Saurer, M., Siegwolf, R.T., Schweingruber, F.H., 2004. Carbon isotope discrimination indicates improving water-use efficiency of trees in northern Eurasia over the last 100 years. Glob. Chang. Biol. 10, 2109–2120.

Scharnweber, T., Heubner, K.-U., Smiljanic, M., Heinrich, I., van der Maaten-Theunissen, M., Struwe, T., Buras, A., Wilmking, M., 2019. Removing the no-analogue bias in modern accelerated tree growth leads to stronger medieval drought. Sci. Rep. 9 https://doi.org/10.1038/s41598-019-39040-5.

Silva, L., Anand, M., 2013. Probing for the influence of atmospheric CO2 and climate change on forest ecosystems across biomes. Glob. Ecol. Biogeogr. 22, 83–92.

Silva, L., Horwath, W., 2013. Explaining global increases in water use efficiency: why have we overestimated responses to rising atmospheric CO2 in natural forest ecosystems? PLoS One 8, e53089.

Song, L., Zhu, J., Zhang, J., Wang, KLü L., Wang, F., Wang, G., 2019. Divergent growth responses to warming and drying climates between native and non-native tree species in Northeast China. Trees 33, 1143–1155.

Soule, P., Knapp, P., 2006. Radial growth rate increases in naturally occurring ponderosa pine trees: a late-20th century CO2 fertilization effect? New Phytol. 171, 379–390.

Steinhilber, F., Abreu, J.A., Beer, J., Brunner, I., Christl, M., Fischer, H., 2012. 9,400 years of cosmic radiation and solar activity from ice cores and tree rings. Proc. Natl. Acad. Sci. 1–5. https://doi.org/10.1073/pnas.1118965109.

Stokes, M., Smiley, T., 1968. An Introduction to Tree-Ring Dating. The University of Chicago Press.

Stott, P., Jones, G.S., 2009. Variability of high latitude amplification of anthropogenic warming. Geophys. Res. Lett. 36, 1–6.

Strelin, J.A., Kaplan, M., Vandergoes, M.J., Denton, G.H., Schaefer, J.M., 2014. Holocene glacier history of the Lago Argentino basin, southern Patagonian icefield. Quat. Sci. Rev. 101, 124–145.

Tierney, J., Abram, N., Anchukaitis, K., Evans, M., Giry, C., Kilbourne, K., Saenger, C., Wu, H., Zinke, J., 2015. Tropical sea surface temperatures for the past four centuries reconstructed from coral archives. Paleoceanography 30, 226–252.

Torrence, C., Compo, G.P., 1998. A practical guide to wavelet analysis. Bull. Am. Meteorol. Soc. 79, 61–78.

Trenberth, K., Fasullo, J.T., Branstator, G., Phillips, A.S., 2014. Seasonal aspects of the recent pause in surface warming. Nat. Clim. Chang. 4, 911–916. https://doi.org/10.1038/NCLIMATE2341.

Urrutia-Jalabert, R., Malhi, Y., Barichivich, J., Lara, A., Delgado-Huertas, A., Rodríguez, C.G., Cuq, E., 2015a. Increased water use efficiency but contrasting tree growth patterns in Fitzroya cupressoides forests of southern Chile during recent decades. J. Geophys. Res. Biogeosci. 120, 2505–2524. https://doi.org/10.1002/2015JG003098.

Urrutia-Jalabert, R., Malhi, Y., Lara, A., 2015b. The oldest , slowest rainforests in the World ? Massive biomass and slow carbon dynamics of Fitzroya cupressoides temperate forests in. PLoS One 1–24. https://doi.org/10.1371/journal.pone.0137569.

Villalba, R., 1990. Climatic fluctuations in northern Patagonia during the last 1000 years as inferred from tree-ring records. Quat. Res. 34, 346–360.

Villalba, R., Boninsegna, J.A., Lara, A., Veblen, T., Roig, F., Aravena, J.C., Ripalta, A., 1996. Interdecadal climatic variations in millennial temperature reconstructions from Southern South America. In: Jones, P.D., Bradley, R., Jouzel, J. (Eds.), Climatic Variations and Forcing Mechanisms of the Last 2000 Years. Springer, Berlin, pp. 161–189.

Villalba, R., Lara, A., Boninsegna, J., Masiokas, M., Delgado, S., Aravena, J.C., Roig, F.A., Schmelter, A., Wolodarsky, A., Ripalta, A., 2003. Large-scale temperature changes across the southern Andes: 20th-century variations in the context of the past 400 years. In: Díaz, H.F. (Ed.), Climate Variability and Change in High Elevation Regions: Past, Present & Future. Advances in Global Change Research. Springer, Dordrecht, pp. 177–232.

Villalba, R., Lara, A., Masiokas, M., Urrutia, R., Luckman, B., Marshall, G., Mundo, I., Christie, D., Cook, E., Neukom, R., Allen, K., Fenwick, P., Boninsegna, J., Srur, A., Morales, M., Araneo, D., Palmer, J., Cuq, E., Aravena, J., Holz, A., Lequesne, C., 2012. Unusual southern hemisphere tree growth patterns induced by changes in the southern annular mode. Nat. Geosci. 5, 793–798. https://doi.org/10.1038/ngeo1613.

Vuille, M., Franquist, E., Garreaud, R., Lavado Casimiro, W.S., Cáceres, B., 2015. Impact of the global warming hiatus on Andean temperature. J. Geophys. Res. Atmos. 120 https://doi.org/10.1002/2015JD023126.

Wigley, T.M., Briffa, K.R., Jones, P.D., 1984. On the average value of correlated time series, with applications in dendroclimatology and hydrometeorology. J. Appl. Meteorol. Climatol. 23, 201–213.

Wilson, R., Anchukaitis, K., Briffa, K.R., Büntgen, U., Cook, E., Arrigo, R.D., Davi, N., Esper, J., Frank, D., Hegerl, G., Helama, S., Klesse, S., Krusic, P.J., Linderholm, H.W., Myglan, V., Osborn, T.J., Zhang, P., Zorita, E., Schurer, A., Wiles, G., 2016. Last millennium northern hemisphere summer temperatures from tree rings : Part I : the long term context. Quat. Sci. Rev. 134, 1–18. https://doi.org/10.1016/j.quascirev.2015.12.005.